IEEE Access
Multidisciplinary | Rapid Review | Open Access Journal

Received February 7, 2022, accepted February 20, 2022, date of publication February 22, 2022, date of current version March 4, 2022.

Digital Object Identifier 10.1109/ACCESS.2022.3153839

Synchronous Control of 2-D.O.F Master-Slave Manipulators Using Actuators With Asymmetric Nonlinear Dead-Zone Characteristics

DAEYI JUNG AND JONGYEON JEON
School of Mechanical and Automotive Engineering, Kunsan National University, Gunsan 54150, South Korea

Corresponding author: Daeyi Jung (dyjung@kunsan.ac.kr)

This work was supported in part by the Competency Development Program for Industry Specialists of Korean Ministry of Trade, Industry and Energy (MOTIE), operated by the Korea Institute for Advancement of Technology (KIAT) (HRD Program for Future Car) under Grant N0002428; and in part by the KIAT Grant funded by the Korea Government (MOTIE) (The Competency Development Program for Industry Specialist) under Grant P0012769.

ABSTRACT Although the various synchronous control techniques of a master-slave manipulator have been explored and developed over the decades, the investigations of the synchronous control for those systems with strong asymmetric dead-zone characteristics have been limited and not been fully considered. Hence, we proposed the robust and easy-to-implement estimation and control strategy to compensate for the actuator's dead-zone effect and to guarantee synchronous performance. Specifically, we set up a two-step process called prior-estimation control to avoid the performance degradation due to the frequent failures of the desired estimation in a standard adaptive control. The first step is to adaptively estimate the asymmetric nonlinear dead-zone parameters via the Recursive Least Square (RLS) method. At the second stage, those estimated parameters via RLS are delivered to the main synchronous control system designed by a passivity-based sliding mode control technique along with inverse dead-zone control, and then the control is executed whenever a human operator interacts with the system. Finally, the effectiveness of the proposed approach has been validated by the actual 2-D.O.F master-slave manipulators equipped with cost-effective actuators with an inevitable asymmetric dead-zone. This work will be especially a valuable asset for those who wish to accurately control the master-slave systems with dead-zone characteristics such as the industrial construction multiple joints based fork cranes or lifts.

INDEX TERMS Master-slave manipulator, dead-zone (DZ), inverse dead-zone control (IDZ), passivity-based sliding mode control, recursive least square (RLS).

I. INTRODUCTION

Over the years, various synchronous control strategies of master-slave manipulators have been investigated and developed. In particular, approaches such as PD/PID control, robust/adaptive control, adaptive neural networks, and combined solutions with the concept of energy passivity have been considered to solve this problem.

Early but still pioneering and valuable works using an observer-controller scheme, passive decomposition, a force symmetry bilateral control strategy and, an impedance identifier are presented in [1]–[9]. [1] presented experimental results for master-slave synchronization of two robotic manipulators based on the observer-controller scheme. Especially, the uniform ultimate boundedness of the synchronization errors is addressed here. [2] proposed the hydraulic servo 6-DOF master-slave Stewart platform and presented the so-called force symmetry bilateral servo control strategy that improves the response rate and tele-presence of the master-slave control system. [3] explored the slave robot of the macro-micro tele-operation system including 1-DOF piezo actuator with hysteresis nonlinearity. Here, the LuGre friction model is employed to estimate the hysteresis loop and passive decomposition has been applied to design the control system. [4] proposed a new bilateral control scheme to guarantee the stability of tele-operation system. Specifically, the passivity observer and controller achieve the stable tele-operation under conditions such as hard wall contact and following. [5] investigated a passive bilateral feed-forward control scheme for linear dynamically similar (LDS) tele-operated

The associate editor coordinating the review of this manuscript and approving it for publication was Jinquan Xu.

master-slave manipulator with kinematic and power scaling. The proposed technique is robust for model uncertainty and inaccuracy of force measurement and individually secures the aspects for the coordination error and overall motion. Furthermore, [6] proposed a passive bilateral tele-operation control law for the multiple DOF nonlinear master-slave robotic systems. The main innovation used here is the passive decomposition for 2n-DOF nonlinear tele-operated dynamics without contravening passivity. [7] presents a novel control framework for the nonlinear master-slave robotic systems under the constant communication delays. Utilizing the passivity controller, Lyapunov-Krasovskii technique, as well as Paeseval's identity, this work shows that the combination of constant delayed communication and control are altogether passive and robust. [8] proposed a new approach using the optimal 4-channel architecture in aspect of transparency in tele-operation, which is capable of providing ideal transparency under the communication delays. [9] presents a master-slave control method based on the identifications of load force and impedance for Tele-operated hydraulic construction robotic system which is composed of a hydraulic excavator and two joysticks. Here, the load force and impedance identifiers are used for identifying the load force and impedance of the slave actuator respectively.

Furthermore, even though early works [1]–[9] successfully guarantees the performance of master-slave operation, to strengthen the robustness and adaptability of between tele-operating systems and human operators, several works [10]–[17] adopt more advanced control methods such as the sliding mode control approaches and adaptive techniques together with fuzzy technique. [10] proposed a control strategy based on sliding mode control for master-slave manipulator control system. This proposed approach achieves the excellent performance on force and position tracking for the master and slave manipulator. [11] addresses a master–slave synchronous strategy for complex dynamic systems based on feedback control which obtains the matching in such complicated as chaotic motions of end-effectors. [12] claims the master–slave control strategy for a novel surgical robot for MIS. Here, the control strategy in Cartesian space handles with the problems of kinematics transformation on consistency principle, intra-operative re-mapping and tremor attenuation in real-time. [13] proposed a model-free controller that combines simplicity of PD control with robustness of sliding mode control (so-called PD-ISMC (Integral Sliding Mode Control)). The robust trajectory tracking performance was verified by using the actual surgeon's surgical motion data and implementing master-slave system. Using an adaptive neural network control, [14] investigated for single-master-multiple-slaves tele-operation in consideration of time delays and input dead-zone uncertainties for multiple mobile manipulators carrying a common object in a cooperative manner. [15] presented a novel bilateral control scheme without force sensors for a 3-D.O.F hydraulic servo system with master–slave manipulators. The sliding mode control with sliding perturbation observer (SMCSPO) using a bilateral control environment are used to achieve bilateral controller for the robust position tracking and control of the slave device. The sliding perturbation observer (SPO) estimates the reaction force at the end effecter without using any sensors. The sliding mode control (SMC) is used as a bilateral controller for the robust position tracking and control of the slave device. [16] considered tele-operated flexible master and slave systems. Based on the partial differential equations based dynamic model, a bilateral coordination controller is developed to achieve the coordination angle tracking and vibration suppression of inherent flexibility in master–slave manipulators. Finally, the system is proven to be asymptotically stable via a given control. [17] describes a globally stable adaptive fuzzy back-stepping control for nonlinear bilateral tele-operation manipulators to accomplish the great transparency performance of both position tracking and force feedback under communication delay.

More recently, rather than model based approaches in [10]–[19], adaptive neural network techniques (i.e, model free approach) have been applied to the master-slave system to guarantee telepresence performance [18]–[20]. [18] includes a radial basis function (RBF) neural network based adaptive robust control design to cope with the communication time delay, various nonlinearities, and uncertainties of manipulator. Specifically, the slave environmental dynamics is modeled by a general RBF neural network for the environmental torque reconstruction in the master side. [19] explores the ANN based novel trajectory tracking control strategies for trilateral tele-operation systems with Dual-master/Single-slave robot manipulators under communication constant time delays. [20] presents a flatted neural network based admittance control scheme for robotic manipulators in the presence of the actuator dead-zone without using force sensing. Here, an experiment using the Baxter robot has been implemented to evaluate the effectiveness of the proposed technique.

Along with tele-operation robotics systems, the control scheme for the actuators (such as a geared motor) with uncertain dead-zone nonlinearity induced by a gear backlash and imperfectly manufactured mechanical parts has been developed for a long times. The related works [21]–[27] utilized the inverse of dead-zone, adaptive estimation/control, and neural network to overcome dead-zone effect. [21] presents nonlinear modeling and identification of a DC motor rotating in two directions and verified the accuracy of proposed technique based on real time experiments. Here, online parameter identification is executed using the recursive least squares method. In [22], a dead-zone compensator is proposed for a DC motor system based on a fuzzy logic controller, guaranteeing small tracking errors and bounded parameter estimates. [23], [24] proposed an adaptive control scheme for systems with uncertain dead-zone nonlinearity. Here, a new model for inverse dead-zone is introduced and utilized in conjunction with any conventional adaptive controllers (i.e, simultaneous control and estimation) to minimize the effect of dead-zone. [25] focused on hybrid model predictive control (MPC) for dealing with asymmetric dead-zone and

shows that the proposed control strategy is superior to the standard MPC approach. [26] presented an adaptive control approach based on the two neural networks to control a DC motor system with dead-zone characteristics (DZC). [27] employed a differential neural network in order to identify the uncertain dynamics with unknown dead-zone which is modeled as a combination of a linear term and a disturbance-like term. Here, the Lyapunov analysis is used to show asymptotic converge of the identification error to a bounded zone. Furthermore, it shows that the difference between the state of the neural identifier and the reference trajectory converges exponentially to zero. Although the various control strategies [1]–[10], [13]–[15], [17]–[20] of a master-slave manipulator have been developed for many applications so far, the studies of synchronous control for higher DOF nonlinear master-slave manipulator systems incorporating actuators with nonlinear dead-zone characteristics have been limited and several existing results are complicate to be implemented in industrial application. In addition, even though the recent approaches based on the adaptive neural networks [17]–[20] are promising for master-slave system with dead-zone effect, those are still challenging to be applied to the cost-effective commercial manipulator due to the limitation of micro-controller. Hence, this paper proposed the compact and effective estimation-control strategy to disengage the asymmetric dead-zone effect for the precise synchronous control between the master and the slave. Here, a two-stage approach has been proposed: In the first stage, the primary dead-zone parameters are estimated through Recursive Least Square method together with PD-control to track a given desired trajectories without a human's intervention. Here, rather than the complicate estimation methods used in [22]–[27], the modified approach for estimating the asymmetric feature of dead-zone has been proposed based on standard RLS in [21]. On the other hand, at the second stage, those estimated parameters obtained from the first stage are delivered to the main controller designed by passivity-based sliding mode control (SMC) based on the idea of passive decomposition [4]–[6] and the technique of SMC [13]–[15], and then the proposed synchronization control (i.e, asymmetric dead-zone compensation and SMC) is activated. The reason for selecting a two-stage approach instead of a standard adaptive control approach (i.e. simultaneous estimation and control) is owing to the fact that a failure in system control is inevitable once an adaptive estimation is unsuccessfully performed as possibly seen from [23], [24].

Based on an actually fabricated experimental setup, the effectiveness of proposed control strategy has been verified in the aspects of tele-presence. This work will contribute to developing a precise position control strategy of the master-slave system using the cost-effective motor/actuator. The rests of paper are followed. **Sec.II** presents the 2-DOF mathematical model of master-slaver manipulator system while **Sec.III** introduces the estimation of dead-zone parameters via RLS. **Sec.IV** proposed the passivity-based sliding mode control design and **Sec.V** discussed experimental results. Finally, the conclusions are remarked.

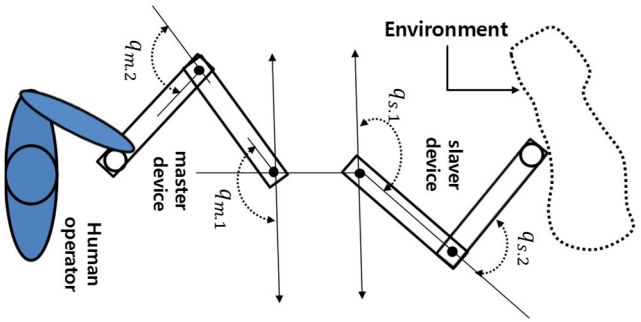

FIGURE 1. General feature of 2-DOF master-slaver manipulator.

II. 2-D.O.F MASTER-SLAVE MANIPULATOR SYSTEM

This section introduces the mathematical model of 2-DOF master and slave manipulators which is dynamically identical to each other. And, the general feature of the target system is described in Fig.1. Consider the equations of motions (EOM) for both master and slave manipulators,

$$\boldsymbol{M_m}\left(\boldsymbol{q_m}\right)\ddot{\boldsymbol{q}}_{\boldsymbol{m}}+\boldsymbol{C_m}\left(\boldsymbol{q_m},\dot{\boldsymbol{q}}_{\boldsymbol{m}}\right)\dot{\boldsymbol{q}}_{\boldsymbol{m}} = \mathrm{DZ_m}(\boldsymbol{\tau_m}(t))+\mathbf{T_h}(t) \quad (1)$$

$$\boldsymbol{M_s}\left(\boldsymbol{q_s}\right)\ddot{\boldsymbol{q}}_{\boldsymbol{s}}+\boldsymbol{C_s}\left(\boldsymbol{q_s},\dot{\boldsymbol{q}}_{\boldsymbol{s}}\right)\dot{\boldsymbol{q}}_{\boldsymbol{s}} = \mathrm{DZ_s}(\boldsymbol{\tau_s}(t)) + \mathbf{T_E}(t) \quad (2)$$

The corresponding coordinates of systems are defined as,

$$\boldsymbol{q_m} = \begin{bmatrix} q_{m.1} & q_{m.2}\end{bmatrix}^{\mathrm{T}} \in \mathbb{R}^{2\times 1} \;\&\; \boldsymbol{q_s} = \begin{bmatrix} q_{s.1} & q_{s.2}\end{bmatrix}^{\mathrm{T}} \in \mathbb{R}^{2\times 1} \quad (3)$$

where $q_{m.1}$ and $q_{m.2}$ are the angular positions of the first and second joints in the master device while $q_{s.1}$ and $q_{s.2}$ indicate the angular positions of the first and second joints in the slave. Also, $\boldsymbol{M_m}(\boldsymbol{q_m}) \in \mathbb{R}^{2\times 2}$ and $\boldsymbol{M_s}(\boldsymbol{q_s}) \in \mathbb{R}^{2\times 2}$ are the positive-definite and symmetric mass matrices of master and slave system. And, $\boldsymbol{C_m}(\boldsymbol{q_m}, \dot{\boldsymbol{q}}_{\boldsymbol{m}}) \in \mathbb{R}^{2\times 2}$ and $\boldsymbol{C_s}(\boldsymbol{q_s}, \dot{\boldsymbol{q}}_{\boldsymbol{s}}) \in \mathbb{R}^{2\times 2}$ represent the skew-symmetric Coriolis matrices satisfying $\dot{\boldsymbol{M}}_{\boldsymbol{i}}\left(\boldsymbol{q_i}\right)-2\boldsymbol{C_i}(\boldsymbol{q_i}, \dot{\boldsymbol{q}}_{\boldsymbol{i}})$ for $i = m, s$ (i.e, master and slave) while $\boldsymbol{\tau_m}(t) = \begin{bmatrix} \tau_{m.1} & \tau_{m.2}\end{bmatrix}^{\mathrm{T}} \in \mathbb{R}^{2\times 1}$ and $\boldsymbol{\tau_s}(t) = \begin{bmatrix} \tau_{s.1} & \tau_{s.2}\end{bmatrix}^{\mathrm{T}} \in \mathbb{R}^{2\times 1}$ do the torque generated by actuators in the system. Also, $\mathbf{T_h}(t) = \begin{bmatrix} 0 & \mathrm{T}_h\end{bmatrix}^{\mathrm{T}} \in \mathbb{R}^{2\times 1}$ and $\mathbf{T_E}(t) = \begin{bmatrix} 0 & \mathrm{T}_E\end{bmatrix}^{\mathrm{T}} \in \mathbb{R}^{2\times 1}$ are a torque delivered by a human operator and one generated from an environment contacting with the slave device (i.e, end-effectors). It is generally known that T_h and T_E are bounded such as $|\mathrm{T}_h| \le \rho_1 \in \mathbb{R}$ and $|\mathrm{T}_E| \le \rho_2 \in \mathbb{R}$ and passive since the mechanical master-slave system satisfies the energetic passivity condition [5], [6]. $\mathrm{DZ_m}(\cdot)$ and $\mathrm{DZ_s}(\cdot)$ indicate the dead-zone effect of actuator which will be discussed in the next Sec.

III. ONLINE ADAPTIVE ESTIMATION OF DEAD-ZONE PARAMETERS VIA RLS

Due to gear backlash and imperfectly manufactured mechanical parts, the asymmetric dead-zone of actuator (i.e, hysteresis effect) is inevitable. Especially, it is obvious

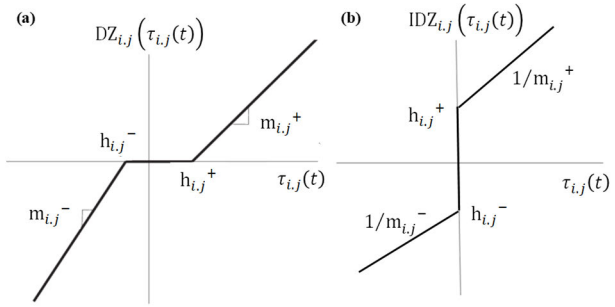

FIGURE 2. Asymmetric dead-zone characteristic and the corresponding inverse dead-zone. (a) asymmetric dead-zone. (b) Inverse dead-zone.

that the cost-effective actuators possess strong dead-zone effect. Hence, this section presents the adaptive estimation strategy of dead-zone effect for each actuator (i.e, a geared D.C electrical motor) based on Recursive Least Square (RLS) method designed for separate estimation in both directional rotations (i.e CCW/CW). This estimation process will be conducted without the intervention of a human operator in the manner that the system automatically searches for the desired parameters according to the scenario where the systems is enforced to track the given desired trajectories. Here, it should be emphasized that the accurate estimation of pure dead-zone effect of actuators can be achieved without human interventions and environmental disturbances. Once the estimation is completed, the estimates of dead-zone parameters will be conveyed to the synchronous control (will be discussed in next Sec. (i.e, **Sec.IV**)). Considering the asymmetric nonlinear dead-zone characteristic of the geared-electrical motors for the system,

$$\mathrm{DZ}_{i.j}\left(\tau_{i.j}\left(t\right)\right)=\begin{pmatrix} \mathrm{m}_{i.j}{}^{+}(\tau_{i.j}-\mathrm{h}_{i.j}{}^{+}) & \text{if } \tau_{i.j}>\mathrm{h}_{i.j}{}^{+} \\ 0 & \text{if } -\mathrm{h}_{i.j}{}^{-}\le\tau_{i.j}\le\mathrm{h}_{i.j}{}^{+} \\ \mathrm{m}_{i.j}{}^{-}(\tau_{i.j}+\mathrm{h}_{i.j}{}^{-}) & \text{if } \tau_{i.j}<-\mathrm{h}_{i.j}{}^{-} \end{pmatrix} \quad \text{for } i=m,s \text{ and } j=1,2 \tag{4}$$

Here, $\mathrm{m}_{i.j}{}^{+}$ and $\mathrm{m}_{i.j}{}^{-}$ are the unknown distorted slopes of dead-zone for the positive input (i.e, $\tau_{i.j}>0$) and the negative one (i.e, $\tau_{i.j}<0$) respectively. On the other hands, $\mathrm{h}_{i.j}{}^{+}$ ($\tau_{i.j}>0$) and $\mathrm{h}_{i.j}{}^{-}$ ($\tau_{i.j}<0$) represent the unknown distorted offsets of dead-zone. The sub-notation i in (4) indicates the master and the slave while the j represents the 1st and 2nd actuators in each system.

Also, based on (4), the inverse dead-zone (i.e, counteraction for Dead-Zone) can be formulated as,

$$\mathrm{IDZ}_{i.j}\left(\tau_{i.j}\left(t\right)\right)=\begin{pmatrix} 1/\mathrm{m}_{i.j}{}^{+}\tau_{i.j}+\mathrm{h}_{i.j}{}^{+} & \text{if } \tau_{i.j}>0 \\ 1/\mathrm{m}_{i.j}{}^{-}\tau_{i.j}-\mathrm{h}_{i.j}{}^{-} & \text{if } \tau_{i.j}<0 \end{pmatrix} \quad \text{for } i=m,s \text{ and } j=1,2 \tag{5}$$

Based on (4) and (5), the general characteristics of asymmetric dead-zone and the corresponding inverse dead-zone are described in Fig.2.

Next, recalling that no human intervention in the master and external forces/torques in the slave are presented during the first step (i.e, $\mathbf{T_h}\left(t\right)=\mathbf{0}$ and $\mathbf{T_E}\left(t\right)=\mathbf{0}$), the (1) and (2) can be expressed by,

$$\begin{bmatrix} M_{i.11}(\boldsymbol{q_i}) & M_{i.12}(\boldsymbol{q_i}) \\ M_{i.21}(\boldsymbol{q_i}) & M_{i.22}(\boldsymbol{q_i}) \end{bmatrix}\begin{bmatrix} \ddot{q}_{i.1} \\ \ddot{q}_{i.2} \end{bmatrix} + \begin{bmatrix} C_{i.11}(\boldsymbol{q_i},\dot{\boldsymbol{q}}_{\boldsymbol{i}}) & C_{i.12}(\boldsymbol{q_i},\dot{\boldsymbol{q}}_{\boldsymbol{i}}) \\ C_{i.21}(\boldsymbol{q_i},\dot{\boldsymbol{q}}_{\boldsymbol{i}}) & C_{i.22}(\boldsymbol{q_i},\dot{\boldsymbol{q}}_{\boldsymbol{i}}) \end{bmatrix}\begin{bmatrix} \dot{q}_{i.1} \\ \dot{q}_{i.2} \end{bmatrix} = \cdots\cdots = \begin{bmatrix} \mathrm{DZ}_{i.j}(\tau_{i.1}) \\ \mathrm{DZ}_{i.j}(\tau_{i.2}) \end{bmatrix} \text{ for } i=m,s \tag{6}$$

To estimate the dead-zone parameters for the systems in (6), the following regression models are suggested by,

$$y_{i.j}{}^{(\pm)}(\mathrm{k}) = \left[\boldsymbol{\Phi}_{i.j}{}^{(\pm)}\left(\mathrm{k}-1\right)\right]^{\mathrm{T}}\boldsymbol{\Theta}_{i.j}{}^{(\pm)}(\mathrm{k}-1) \quad \text{for } i=m,s \text{ and } j=1,2 \tag{7}$$

The detail of each component in (7) is given by,

$$y_{i.j}{}^{(\pm)}(\mathrm{k}) = M_{i.j1}(\boldsymbol{q_i})\ddot{q}_{i.1} + M_{i.j2}(\boldsymbol{q_i})\ddot{q}_{i.2} + C_{i.j1}(\boldsymbol{q_i},\dot{q}_{\boldsymbol{i}})\dot{q}_{i.1} + C_{i.j2}(\boldsymbol{q_i},\dot{\boldsymbol{q}}_{\boldsymbol{i}})\dot{q}_{i.2} \in \mathbb{R} \tag{8}$$

$$\left[\boldsymbol{\Phi}_{i.j}{}^{(\pm)}(\mathrm{k}-1)\right]^{\mathrm{T}} = [\tau_{i.j}\left(t\right) \mp 1] \in \mathbb{R}^{1\times 2} \tag{9}$$

$$\boldsymbol{\Theta}_{i.j}{}^{(\pm)}(\mathrm{k}-1) = [\mathrm{m}_{i.j}{}^{(\pm)}\left(\mathrm{m}_{i.j}\mathrm{h}_{i.j}\right)^{(\pm)}] \in \mathbb{R}^{2\times 1} \tag{10}$$

Here, the upper sub-notations $(\pm)$ indicates either $+$ or $-$ determined by the sign of input torques $\tau_{i.j}$ (i.e, $\tau_{i.j}>0$ (positive) or $\tau_{i.j}<0$ (negative)). Therefore, depending on the sign of $\tau_{i.j}$, the separate estimations can be performed based on the proposed schemes in (7) through (10). This implies that we can secure the estimates of asymmetric featured dead-zone.

The unknown vector parameters $\boldsymbol{\Theta}_{i.j}{}^{(\pm)}(k)$ is recursively obtained by,

$$\boldsymbol{L}_{i.new}(k) = \boldsymbol{P}_{i.j}{}^{(\pm)}(\mathrm{k}-1)\boldsymbol{\Phi}_{i.j}{}^{(\pm)}(\mathrm{k}-1)/H_{i.j}(\mathrm{k}) \in \mathbb{R}^{2\times 1} \tag{11}$$

$$\boldsymbol{P}_{i.j}(\mathrm{k}) = \frac{\boldsymbol{P}_{i.j}{}^{(\pm)}(\mathrm{k}-1)}{\lambda}\left(\boldsymbol{I}_{2\times 2}-\boldsymbol{L}_{i.new}(\mathrm{k})\left[\boldsymbol{\Phi}_{i.j}{}^{(\pm)}(\mathrm{k})\right]^{T}\right) \in \mathbb{R}^{2\times 2} \tag{12}$$

$$\boldsymbol{\Theta}_{i.j}{}^{(\pm)}(\mathrm{k}) = \boldsymbol{\Theta}_{i.j}{}^{(\pm)}(\mathrm{k}-1) + \boldsymbol{L}_{i.new}(\mathrm{k})E_{i.j}(\mathrm{k}) \in \mathbb{R}^{2\times 1} \tag{13}$$

$H_{i.j}(\mathrm{k})$ and $E_{i.j}(\mathrm{k})$ in (11) through (13) are computed by,

$$H_{i.j}(\mathrm{k}) = \lambda+\left[\boldsymbol{\Phi}_{i.j}{}^{(\pm)}\left(\mathrm{k}-1\right)\right]^{T}\boldsymbol{P}_{i.j}{}^{(\pm)}(\mathrm{k}-1)\boldsymbol{\Phi}_{i.j}{}^{(\pm)}(\mathrm{k}-1) \in \mathbb{R} \tag{14}$$

$$E_{i.j}(\mathrm{k}) = \left(y_{i.j}{}^{(\pm)}(\mathrm{k}) - \left[\boldsymbol{\Phi}_{i.j}{}^{(\pm)}\left(\mathrm{k}-1\right)\right]^{T}\boldsymbol{\Theta}_{i.j}{}^{(\pm)}(\mathrm{k}-1)\right) \in \mathbb{R} \tag{15}$$

where $\lambda\in\mathbb{R}$ is the positive forgetting factor of estimation and the notation k represents the time-step of estimation process.

The PD-based control is used to perform the estimation of dead-zone parameters as followed by,

$$\boldsymbol{\tau}_{i.j}\left(t\right) = \boldsymbol{M_i}\left(\boldsymbol{q_i}\right)\ddot{\boldsymbol{q}}_{\boldsymbol{i.d}} + \boldsymbol{C_i}\left(\boldsymbol{q_i},\dot{\boldsymbol{q}}_{\boldsymbol{i}}\right)\dot{\boldsymbol{q}}_{\boldsymbol{i}} - \boldsymbol{C}_{\mathbf{D}.\boldsymbol{i}}\left(\dot{\boldsymbol{q}}_{\boldsymbol{i}}-\dot{\boldsymbol{q}}_{\boldsymbol{i.d}}\right) - \mathbf{K}_{\mathbf{p}.\boldsymbol{i}}\left(\boldsymbol{q_i}-\boldsymbol{q}_{\boldsymbol{i.d}}\right) \in \mathbb{R}^{2\times 1} \text{ for } i=m,s \tag{16}$$

Initiate Estimation process

Input: Desired trajectory $q_{i.\mathrm{d}}$

Do PD-based Control of system
Estimate dead-zone parameters using RLS
while (Norm of covariance $\|P_{i.j}(k)\| <$ ep)

return Estimated Parameters $\left[\mathrm{m}_{i.j}{}^{(\pm)} \quad (\mathrm{m}_{i.j}\mathrm{h}_{i.j})^{(\pm)}\right]$

Terminate Estimation Process

FIGURE 3. Adaptive estimation of dead-zone parameters via RLS together with PD-based control.

where, $\boldsymbol{C}_{\mathbf{D}.i} > \mathbf{0} \in \mathbb{R}^{2\times2}$ and $\mathbf{K}_{\mathbf{p}.i} > \mathbf{0} \in \mathbb{R}^{2\times2}$ for $i = m, s$ are the diagonal positive constant gain matrices. Also, $\boldsymbol{q}_{i.\mathbf{d}} = \left[\mathrm{A}_i \sin(\omega_i t)\ \mathrm{A}_2 \sin(\omega_i t)\right]^T \in \mathbb{R}^{2\times1}$ is the desired sinusoidal trajectory and A_i, ω_i, and t are the maximum amplitudes, the frequencies and a time respectively. In other words, the estimation of parameters is conducted while the system is actuated to track the given $\boldsymbol{q}_{i.\mathbf{d}}$. The estimation will be terminated if the norm of covariance matrices $\|\boldsymbol{P}_{i.j}(k)\|$ is sufficiently small. To provide a clear understanding of the entire estimation strategy, a brief pseudo code of dead zone parameter estimation via RLS together with PD-based control is shown in Fig.3.

IV. PASSIVITY-BASED SLIDING MODE CONTROL DESIGN

This section claims the passivity-based sliding mode control design for precise synchronous control of the master-slaver system. The control strategy presented here utilizes the energetically passivity-based technique in conjunction with the estimated parameters obtained from the previous section (i.e, **Sec.III**), resulting in a perfect synchronization between systems using asymmetric dead-zone characteristic actuators.

First, dividing the control input of (1) and (2) into the two entities such that,

$$\boldsymbol{\tau}_{\mathbf{m}}(t) = \boldsymbol{\tau}_{\mathbf{m}.1}(t) + \boldsymbol{\tau}_{\mathbf{m}.2}(t) \tag{17}$$
$$\boldsymbol{\tau}_{\mathbf{s}}(t) = \boldsymbol{\tau}_{\mathbf{s}.1}(t) + \boldsymbol{\tau}_{\mathbf{s}.2}(t) \tag{18}$$

To eliminate the Coriolis effect and nonlinear terms, let the second part of control law in (17) and (18) be chosen as,

$$\boldsymbol{\tau}_{\mathbf{m}.2}(t) = \Delta\boldsymbol{M}_m(\boldsymbol{q}_m)\ddot{\boldsymbol{q}}_m + \boldsymbol{C}_m(\boldsymbol{q}_m, \dot{\boldsymbol{q}_m})\dot{\boldsymbol{q}_m} \tag{19}$$
$$\boldsymbol{\tau}_{\mathbf{s}.2}(t) = \Delta\boldsymbol{M}_s(\boldsymbol{q}_s)\ddot{\boldsymbol{q}}_s + \boldsymbol{C}_s(\boldsymbol{q}_s, \dot{\boldsymbol{q}}_s)\dot{\boldsymbol{q}}_s \tag{20}$$

where, $\Delta\boldsymbol{M}_m(\boldsymbol{q}_m) = \boldsymbol{M}_m(\boldsymbol{q}_m) - \boldsymbol{M}_{m.c} \in \mathbb{R}^{2\times2}$ and $\Delta\boldsymbol{M}_s(\boldsymbol{q}_s) = \boldsymbol{M}_s(\boldsymbol{q}_s) - \boldsymbol{M}_{s.c} \in \mathbb{R}^{2\times2}$. It is possible that the mass matrices can be decomposed into the nonlinear varying parts and constant ones. Therefore, the matrices $\boldsymbol{M}_{m.c} \in \mathbb{R}^{2\times2} > 0$ and $\boldsymbol{M}_{s.c} \in \mathbb{R}^{2\times2} > 0$ are selected such that those are the diagonal constant positive definitive matrices.

And then, applying (19) and (20) into (1) and (2), the original dynamics (1) and (2) become,

$$\ddot{\boldsymbol{q}_m} = \boldsymbol{M}_{m.c}{}^{-1}[\boldsymbol{\tau}_{\mathbf{m}.1}(t) + \mathbf{T}_{\mathbf{h}}(t)] \tag{21}$$
$$\ddot{\boldsymbol{q}_s} = \boldsymbol{M}_{s.c}{}^{-1}[\boldsymbol{\tau}_{\mathbf{s}.1}(t) + \mathbf{T}_{\mathbf{E}}(t)] \tag{22}$$

Adding (21) with (22) and multiplying 1/2 to it yield,

$$\ddot{\boldsymbol{q}}_{Lock} = \boldsymbol{\tau}_{Lock} + \boldsymbol{\tau}_{Lock.E} \tag{23}$$
$$\boldsymbol{\tau}_{Lock} = [\boldsymbol{M}_{m.c}{}^{-1}\boldsymbol{\tau}_{\mathbf{m}.1}(t) + \boldsymbol{M}_{s.c}{}^{-1}\boldsymbol{\tau}_{\mathbf{s}.1}(t)]/2 \in \mathbb{R}^{2\times1} \tag{24}$$
$$\boldsymbol{\tau}_{Lock.E} = [\boldsymbol{M}_{m.c}{}^{-1}\mathbf{T}_{\mathbf{h}}(t) + \boldsymbol{M}_{s.c}{}^{-1}\mathbf{T}_{\mathbf{E}}(t)]/2 \in \mathbb{R}^{2\times1} \tag{25}$$

where the coordinate $\boldsymbol{q}_{Lock} = (\boldsymbol{q}_m + \boldsymbol{q}_s)/2 \in \mathbb{R}^{2\times1}$ is the locked coordinate which is so-called overall motion of system [5]. Since $\mathbf{T}_{\mathbf{h}}(t)$ and $\mathbf{T}_{\mathbf{E}}(t)$ are bounded such as $\|\mathbf{T}_{\mathbf{h}}(t)\| \le \rho_1 \in \mathbb{R}$ and $\|\mathbf{T}_{\mathbf{E}}(t)\| \le \rho_2 \in \mathbb{R}$, the torque $\boldsymbol{\tau}_{Lock.E}$ in locked coordinate is also bounded such as $\|\boldsymbol{\tau}_{Lock.E}\| \le \delta_{\mathrm{L.E}} \in \mathbb{R}$.

On the other hands, subtracting (22) from (21) yields,

$$\ddot{\boldsymbol{q}}_{shape} = \boldsymbol{\tau}_{shape} + \boldsymbol{\tau}_{shape.E} \tag{26}$$
$$\boldsymbol{\tau}_{shape} = [\boldsymbol{M}_{m.c}{}^{-1}\boldsymbol{\tau}_{\mathbf{m}.1}(t) - \boldsymbol{M}_{s.c}{}^{-1}\boldsymbol{\tau}_{\mathbf{s}.1}(t)] \in \mathbb{R}^{2\times1} \tag{27}$$
$$\boldsymbol{\tau}_{shape.E} = [\boldsymbol{M}_{m.c}{}^{-1}\mathbf{T}_{\mathbf{h}}(t) - \boldsymbol{M}_{s.c}{}^{-1}\mathbf{T}_{\mathbf{E}}(t)] \in \mathbb{R}^{2\times1} \tag{28}$$

where $\boldsymbol{q}_{shape} = (\boldsymbol{q}_m - \boldsymbol{q}_s) \in \mathbb{R}^{2\times1}$ is the shaped coordinate representing the degree of synchronization between the systems. And, it is apparent that $\boldsymbol{\tau}_{shape.E}$ is also bounded such as $\|\boldsymbol{\tau}_{shape.E}\| \le \delta_{\mathrm{S.E}} \in \mathbb{R}$.

Remarks 1. As shown in [6], the control objective is followed. Once $\boldsymbol{q}_{shape} = \boldsymbol{q}_m - \boldsymbol{q}_s \to \mathbf{0}$ is achieved, we can see that $\boldsymbol{q}_{Lock} = 1/2(\boldsymbol{q}_m + \boldsymbol{q}_s) = \boldsymbol{q}_m = \boldsymbol{q}_s$.

Furthermore, proposing the following passivity-based slide mode control (SMC) laws for (23) and (26),

$$\boldsymbol{\tau}_{Lock} = -\boldsymbol{\alpha}_{Lock}(\dot{\boldsymbol{q}}_{Lock}) + \boldsymbol{T}_{Lock.A} \tag{29}$$
$$\boldsymbol{\tau}_{shape} = -\boldsymbol{\alpha}_{shape}\Big[n(\dot{\boldsymbol{q}}_{shape}) + (n\,\boldsymbol{\alpha}_{shape})(\boldsymbol{q}_{shape}) + \boldsymbol{\alpha}_{shape}{}^2\int \boldsymbol{q}_{shape}\,dt\Big] + \boldsymbol{T}_{shape.A} \tag{30}$$

with

$$\mathbf{T}_{Lock.A} = \begin{cases} -\gamma_L \dfrac{\boldsymbol{G}_{Lock}}{\|\boldsymbol{G}_{Lock}\|} & \text{for } \|\boldsymbol{G}_{Lock}\| > \varepsilon_L \\ -\gamma_L \boldsymbol{G}_{Lock}/\varepsilon_L & \text{for } \|\boldsymbol{G}_{Lock}\| \le \varepsilon_L \end{cases} \tag{31}$$

$$\mathbf{T}_{shape.A} = \begin{cases} -\gamma_s \dfrac{\boldsymbol{G}_{shape}}{\|\boldsymbol{G}_{shape}\|} & \text{for } \|\boldsymbol{G}_{shape}\| > \varepsilon_s \\ -\gamma_s \boldsymbol{G}_{shape}/\varepsilon_s & \text{for } \|\boldsymbol{G}_{shape}\| \le \varepsilon_s \end{cases} \tag{32}$$

where, $\boldsymbol{\alpha}_{Lock} \in \mathbb{R}^{2\times2} > 0$ and $\boldsymbol{\alpha}_{shape} \in \mathbb{R}^{2\times2} > 0$ are the diagonal positive constant gain matrices.

And, $n \in \mathbb{R}$, $\gamma_L \in \mathbb{R}$ and $\gamma_s \in \mathbb{R}$ are the positive constants and, ε_L and ε_s are the thickness of boundary layers to prevent the chattering phenomenon.

$\boldsymbol{G}_{Lock}(t)$ and $\boldsymbol{G}_{shape}(t)$ in (31) and (32) represents the designed sliding surfaces and defined as,

$$\boldsymbol{G}_{Lock}(t) = (\dot{\boldsymbol{q}}_{Lock}) \tag{33}$$
$$\boldsymbol{G}_{shape}(t) = (\dot{\boldsymbol{q}}_{shape}) + (n-1)\,\boldsymbol{\alpha}_{shape}(\boldsymbol{q}_{shape}) + \boldsymbol{\alpha}_{shape}{}^2\int \boldsymbol{q}_{shape}\,dt \tag{34}$$

Theorem 1: Based on the proposed control laws in (29) and (30), the system in (23) and (26) are ultimately bounded under the presence of human's intervention and environmental disturbances.

Proof: Applying (29) and (30) into (23) and (26), the corresponding closed-loop system are given by,

$$\dot{\boldsymbol{G}}_{\boldsymbol{Lock}}(t) = -\boldsymbol{\alpha}_{\boldsymbol{Lock}}\boldsymbol{G}_{\boldsymbol{Lock}}(t) + \mathbf{T}_{\boldsymbol{Lock.A}} + \boldsymbol{\tau}_{\boldsymbol{Lock.E}} \quad (35)$$

$$\dot{\boldsymbol{G}}_{\boldsymbol{shape}}(t) = -\boldsymbol{\alpha}_{\boldsymbol{shape}}\boldsymbol{G}_{\boldsymbol{shape}}(t) + \mathbf{T}_{\boldsymbol{shape.A}} + \boldsymbol{\tau}_{\boldsymbol{shape.E}} \quad (36)$$

For the closed-loop system (35) and (36) in each decomposed coordinates, let the candidate Lyapunov functions $V_{Lock}(t)$ and $V_{Shape}(t)$ be,

$$V_{Lock}(t) = \frac{1}{2}\boldsymbol{G}_{\boldsymbol{Lock}}(t)^T\boldsymbol{G}_{\boldsymbol{Lock}}(t) > 0 \quad (37)$$

$$V_{Shape}(t) = \frac{1}{2}\boldsymbol{G}_{\boldsymbol{shape}}(t)^T\boldsymbol{G}_{\boldsymbol{shape}}(t) > 0 \quad (38)$$

The time derivatives of (37) and (38) are given by,

$$\dot{V}_{Lock}(t) = \boldsymbol{G}_{\boldsymbol{Lock}}(t)^T\dot{\boldsymbol{G}}_{\boldsymbol{Lock}}(t) \quad (39)$$

$$\dot{V}_{Shape}(t) = \boldsymbol{G}_{\boldsymbol{shape}}(t)^T\dot{\boldsymbol{G}}_{\boldsymbol{shape}}(t) \quad (40)$$

Furthermore, combining (35) with (39) yields the following consequence,

$$\begin{aligned}\dot{V}_{Lock}(t) &= \Big[\boldsymbol{G}_{\boldsymbol{Lock}}(t)^T\left[-\boldsymbol{\alpha}_{\boldsymbol{Lock}}\boldsymbol{G}_{\boldsymbol{Lock}}(t)\right.\\ &\quad\left.+\mathbf{T}_{\boldsymbol{Lock.A}} + \boldsymbol{\tau}_{\boldsymbol{Lock.E}}\right]\Big]\\ &\le -\boldsymbol{\lambda}_{\boldsymbol{min}}(\boldsymbol{\alpha}_{\boldsymbol{Lock}})\left\|\boldsymbol{G}_{\boldsymbol{Lock}}(t)\right\|^2 + \boldsymbol{G}_{\boldsymbol{Lock}}(t)^T\mathbf{T}_{\boldsymbol{Lock.A}}\\ &\quad + \boldsymbol{G}_{\boldsymbol{Lock}}(t)^T\boldsymbol{\tau}_{\boldsymbol{shape.E}} \quad (41)\end{aligned}$$

where $\boldsymbol{\lambda}_{\boldsymbol{min}}(*) \in \mathbb{R}$ indicates the lowest eigenvalue of a given matrix.

If $\|\boldsymbol{G}_{\boldsymbol{Lock}}\| > \varepsilon_L$,

$$\begin{aligned}\dot{V}_{Lock}(t) &\le -\gamma_L\frac{\boldsymbol{G}_{\boldsymbol{Lock}}(t)^T\boldsymbol{G}_{\boldsymbol{Lock}}}{\|\boldsymbol{G}_{\boldsymbol{Lock}}\|}\\ &\quad + \boldsymbol{G}_{\boldsymbol{Lock}}(t)^T\boldsymbol{\tau}_{\boldsymbol{shape.E}}\\ &\le -\gamma_L\|\boldsymbol{G}_{\boldsymbol{Lock}}\| + \|\boldsymbol{G}_{\boldsymbol{Lock}}\|\left\|\boldsymbol{\tau}_{\boldsymbol{shape.E}}\right\| < 0 \quad (42)\end{aligned}$$

Reminding of $\|\boldsymbol{\tau}_{\boldsymbol{Lock.E}}\| \le \delta_{\mathrm{L.E}}$ and selecting γ_L such as $\delta_{\mathrm{L.E}} < \gamma_L$, we have $\dot{V}_{Lock}(t) \le (\delta_{\mathrm{L.E}} - \gamma_L)\|\boldsymbol{G}_{\boldsymbol{Lock}}\| < 0$.

Similarly, combining (36) with (40) provides,

$$\begin{aligned}\dot{V}_{Shape}(t) &\le \boldsymbol{G}_{\boldsymbol{shape}}(t)^T\left[-\boldsymbol{\alpha}_{\boldsymbol{shape}}\boldsymbol{G}_{\boldsymbol{shape}}(t)\right.\\ &\quad\left.+\mathbf{T}_{\boldsymbol{shape.A}} + \boldsymbol{\tau}_{\boldsymbol{shape.E}}\right]\\ &\le -\boldsymbol{\lambda}_{\boldsymbol{min}}\left(\boldsymbol{\alpha}_{\boldsymbol{shape}}\right)\left\|\boldsymbol{G}_{\boldsymbol{shape}}(t)\right\|^2\\ &\quad + \boldsymbol{G}_{\boldsymbol{shape}}(t)^T\mathbf{T}_{\boldsymbol{shape.A}} + \boldsymbol{G}_{\boldsymbol{shape}}(t)^T\boldsymbol{\tau}_{\boldsymbol{shape.E}}\end{aligned} \quad (43)$$

If $\left\|\boldsymbol{G}_{\boldsymbol{shape}}\right\| > \varepsilon_s$,

$$\begin{aligned}\dot{V}_{Shape}(t) &\le -\gamma_s\frac{\boldsymbol{G}_{\boldsymbol{shape}}{}^T\boldsymbol{G}_{\boldsymbol{shape}}}{\left\|\boldsymbol{G}_{\boldsymbol{shape}}\right\|} + \boldsymbol{G}_{\boldsymbol{shape}}(t)^T\boldsymbol{\tau}_{\boldsymbol{shape.E}}\\ &\le -\gamma_s\left\|\boldsymbol{G}_{\boldsymbol{shape}}\right\| + \left\|\boldsymbol{G}_{\boldsymbol{shape}}\right\|\left\|\boldsymbol{\tau}_{\boldsymbol{shape.E}}\right\|\\ &\le (\delta_{\mathrm{S.E}} - \gamma_s)\left\|\boldsymbol{G}_{\boldsymbol{shape}}\right\| < 0 \quad (44)\end{aligned}$$

Again, recalling of $\left\|\boldsymbol{\tau}_{\boldsymbol{shape.E}}\right\| \le \delta_{\mathrm{S.E}}$ and choosing γ_S such as $\delta_{\mathrm{S.E}} < \gamma_S$ result in $\dot{V}_{Shape}(t) \le (\delta_{\mathrm{S.E}} - \gamma_s)\left\|\boldsymbol{G}_{\boldsymbol{shape}}\right\| < 0$.

Therefore, the overall rate of system (i.e, $\dot{\boldsymbol{q}}_{\boldsymbol{Lock}}$) and the synchronization error between master-slave systems are individually and ultimately bounded as long as $\|\boldsymbol{G}_{\boldsymbol{Lock}}\| > \varepsilon_L$ and $\left\|\boldsymbol{G}_{\boldsymbol{shape}}\right\| > \varepsilon_s$. The proof is completed

The above results also enable us to achieve the condition that the time derivative of total energy is negative (i.e, $\dot{V}_{Lock}(t) + \dot{V}_{Shape}(t) < 0$).

From (24) and (27), the control law in the original coordinates can be obtained using transformation matrix,

$$\begin{bmatrix}\boldsymbol{\tau}_{\mathbf{m.1}}(t)\\ \boldsymbol{\tau}_{\mathbf{s.1}}(t)\end{bmatrix} = \begin{bmatrix}0.5\boldsymbol{M}_{\boldsymbol{m.c}}{}^{-1} & 0.5\boldsymbol{M}_{\boldsymbol{m.s}}{}^{-1}\\ \boldsymbol{M}_{\boldsymbol{m.c}}{}^{-1} & -\boldsymbol{M}_{\boldsymbol{m.s}}{}^{-1}\end{bmatrix}^{-1}\begin{bmatrix}\boldsymbol{\tau}_{\boldsymbol{Lock}}\\ \boldsymbol{\tau}_{\boldsymbol{shape}}\end{bmatrix} \quad (45)$$

Now, combining the 2nd part of control law in (19) and (20), the final control law is given by,

$$\begin{aligned}\begin{bmatrix}\boldsymbol{\tau}_{\mathbf{m}}(t)\\ \boldsymbol{\tau}_{\mathbf{s}}(t)\end{bmatrix} &= \begin{bmatrix}\boldsymbol{\tau}_{\mathbf{m.2}}(t)\\ \boldsymbol{\tau}_{\mathbf{s.2}}(t)\end{bmatrix}\\ &\quad + \begin{bmatrix}0.5\boldsymbol{M}_{\boldsymbol{m.c}}{}^{-1} & 0.5\boldsymbol{M}_{\boldsymbol{m.s}}{}^{-1}\\ \boldsymbol{M}_{\boldsymbol{m.c}}{}^{-1} & -\boldsymbol{M}_{\boldsymbol{m.s}}{}^{-1}\end{bmatrix}^{-1}\begin{bmatrix}\boldsymbol{\tau}_{\boldsymbol{Lock}}\\ \boldsymbol{\tau}_{\boldsymbol{shape}}\end{bmatrix}\end{aligned} \quad (46)$$

Furthermore, applying the inverse-dead zone (i.e, IDZ) control into (46) based on the parameters estimated in Sec.III yields,

$$\begin{bmatrix}\boldsymbol{\tau}_{\mathbf{m.idz}}(t)\\ \boldsymbol{\tau}_{\mathbf{s.idz}}(t)\end{bmatrix} = \begin{bmatrix}\boldsymbol{\alpha}_{\mathbf{m}}{}^{\pm}\boldsymbol{\tau}_{\mathbf{m}}(t) + \boldsymbol{\beta}_{\mathbf{m}}{}^{\pm}\\ \boldsymbol{\alpha}_{\mathbf{s}}{}^{\pm}\boldsymbol{\tau}_{\mathbf{s}}(t) + \boldsymbol{\beta}_{\mathbf{s}}{}^{\pm}\end{bmatrix} \quad (47)$$

$$\begin{aligned}\boldsymbol{\alpha}_{\mathbf{m}}{}^{\pm} &= \begin{bmatrix}1/\mathrm{m}_{\mathrm{m.1}}{}^{(\pm)} & 0\\ 0 & 1/\mathrm{m}_{\mathrm{m.2}}{}^{(\pm)}\end{bmatrix}\ \&\\ \boldsymbol{\alpha}_{\mathbf{s}}{}^{\pm} &= \begin{bmatrix}1/\mathrm{m}_{\mathrm{s.1}}{}^{(\pm)} & 0\\ 0 & 1/\mathrm{m}_{\mathrm{s.2}}{}^{(\pm)}\end{bmatrix}\end{aligned} \quad (48)$$

$$\begin{aligned}\boldsymbol{\beta}_{\mathbf{m}}{}^{\pm} &= \begin{bmatrix}\mathrm{h}_{m.1}{}^{(\pm)} & \mathrm{h}_{m.2}{}^{(\pm)}\end{bmatrix}\ \text{and}\\ \boldsymbol{\beta}_{\mathbf{s}}^{\pm} &= \begin{bmatrix}\mathrm{h}_{s.1}{}^{(\pm)} & \mathrm{h}_{s.1}{}^{(\pm)}\end{bmatrix}\end{aligned} \quad (49)$$

In Fig.4, the pseudo code of entire control scheme is described, which consists of two parts. The first stage indicates the online adaptive estimation (discussed in Sec.III) while the second stage represents the master-slave control in conjunction with a human operator. Specifically, in the first stage, the estimation of dead-zone parameters is performed and then the final converged estimates are delivered to the second stage to destabilize the effect of dead-zone in the actuators. This proposed two-stage process is implemented to achieve better and safer synchronization in master-slave systems.

V. EXPERIMENTAL SETUP AND RESULTS

This section explores the effectiveness of proposed techniques based on actually fabricated 2- D.O.F master-slave manipulators together with a controller(Q-PID-e) and a PC/monitor. As shown in Fig.5, both master and slave devices are individually equipped with two 24V DC-geared motors and the corresponding high resolution encoder (5000 ppr)

Initiate control system

Input: Estimated Dead-zone parameters for inverse dead-zone control
$\left[\mathrm{m}_{i.j}{}^{(\pm)} \quad (\mathrm{m}_{i.j}\mathrm{h}_{i.j})^{(\pm)}\right]$

if a human operator initiates system
Do passivity based sliding mode control and inverse dead-zone control

$$\begin{bmatrix}\boldsymbol{\tau}_{\mathbf{m.idz}}(t)\\ \boldsymbol{\tau}_{\mathbf{s.idz}}(t)\end{bmatrix} = \begin{bmatrix}\boldsymbol{\alpha}_{\mathbf{m}}{}^{\pm}\boldsymbol{\tau}_{\mathbf{m}}(t) + \boldsymbol{\beta}_{\mathbf{m}}{}^{\pm}\\ \boldsymbol{\alpha}_{\mathbf{s}}{}^{\pm}\boldsymbol{\tau}_{\mathbf{s}}(t) + \boldsymbol{\beta}_{\mathbf{s}}{}^{\pm}\end{bmatrix}$$

end if

Terminate Control Process

FIGURE 4. Entire synchronization control scheme.

sensors measuring the angular position of joints in the systems. As shown in Fig.5, it should be noted that the slave device including the motors is an exact replica of the master. Here, we intentionally selected cost-effective geared motors with the highly dead-zone characteristics. The Q-PID-e controller, which is connected to and communicated with the PC/monitor, commands the motions of motors through the D/C motor drivers and reads the rotational angles generated by the encoders based on 200hz frequency. In addition, the proposed control algorithm has been implemented in MATLAB/Simulink and the master device accommodates the handles where a human operator can hold and interact with.

A. ESTIMATION RESULTS OF DEAD-ZONE PARAMETERS

This sub-section presents the estimation results of dead-zone parameters, $\mathrm{m}_{i.j}{}^{(\pm)}$ and $\mathrm{h}_{i.j}{}^{(\pm)}$, based on the technique discussed in Sec.III. Fig.6 shows the desired trajectory of each joint in the master-slave manipulators for estimating the parameters. Based on the PD-control in (16), each link of master and slave devices is enforced to track the desired trajectory, $\boldsymbol{q}_{\boldsymbol{i.d}}$.

In Fig.6, the actual trajectories created by the PD-control are also included together with the errors (i.e, $\boldsymbol{q}_{\boldsymbol{i}} - \boldsymbol{q}_{\boldsymbol{i.d}}$). Considering the angular errors are almost $\pm 8 \sim 9$ degs for the given maximum amplitudes of trajectory, ± 57 degs, it can be seen that the errors are not negligible and the motors employed here are affected by the highly nonlinear dead-zone effect.

Based on the scenario shown in Fig.6, the 4 estimates of $\mathrm{m}_{i.j}{}^{(\pm)}$ and $\mathrm{h}_{i.j}{}^{(\pm)}$ are obtained and shown in both Fig.7 and Fig.8. Fig.7 indicates the estimated parameters representing the distorted slopes $\mathrm{m}_{i.j}{}^{(\pm)}$ while Fig.8 describes the distorted offsets, $\mathrm{h}_{i.j}{}^{(\pm)}$. The results in Fig.7(a) are almost identical to the ones in Fig.7 (c) due to the fact that the identical motors are used for both the 1st joints of master and slave. It is found that the final steady-state values of $\mathrm{m}_{m.1}{}^{(\pm)}$ and $\mathrm{m}_{s.1}{}^{(\pm)}$ are approximately ranging from 0.83 to 0.85, and it shows the $0.15 \sim 0.17$ discrepancies relative to the ideal case, 1 (i.e, no distorted slope). Similarly, the estimated results between Fig.7(b) and Fig.7(d) are well synchronized for each other (i.e, the motors used for the second joints of master and slave devices are identical). The estimated values for $\mathrm{m}_{m.2}{}^{(\pm)}$ and $\mathrm{m}_{s.2}{}^{(\pm)}$ arrived on the values 0.6 and 0.8, respectively. This implies that the motors rotating the second joints-links of systems own the stronger asymmetric dead-zone characteristics compared to the motors attached to the 1st joints of the systems. As predicted by the results in both Fig.7(a) and Fig.7(c), we can also observe that the results in Fig.8(a) are similar to the ones in Fig.8(c). The corresponding final steady-state values of $\mathrm{h}_{m.1}{}^{(\pm)}$ and $\mathrm{h}_{s.1}{}^{(\pm)}$ are approximately 13.1 and 15.2, respectively, which is slightly asymmetrical. Also, the estimated results in Fig.8(b) are well synchronized with the ones in Fig.8(d). The estimated values of both $\mathrm{h}_{m.2}{}^{(\pm)}$ and $\mathrm{h}_{s.2}{}^{(\pm)}$ are respectively 13.2 and 5.73, which can be strongly characterized by the asymmetrical manner. The average of estimated dead-zone parameters, $\mathrm{m}_{i.j}{}^{(\pm)}$ and $\mathrm{h}_{i.j}{}^{(\pm)}$, in both Fig.7 and Fig.8 are summarized in Table.1. According to the results in Fig.7 and Fig.8 together with average values in Table.1, it is apparent that the performance of the proposed estimation strategy is acceptable and consistent.

B. SYNCHRONOUS PERFORMANCE OF PASSIVITY-BASED SLIDING MODE CONTROL WITH IDZ

This sub-section discussed the performance of passivity-based sliding mode control together with IDZ presented in Sec.IV. To investigate the effectiveness of the proposed technique, a human operator is requested to maneuver the handle attached to the second link of the master manipulator, resulting in creating the sine-wave like motion as shown in Fig.9. Here, the estimated dead-zone parameters in the previous sub-section are applied. Fig.9 displays the angular positions of the first joints for master-slave systems ($q_{m.1}$ and $q_{s.1}$), the corresponding error between $q_{m.1}$ and $q_{s.1}$ (i.e, $|q_{m.1} - q_{s.1}|$), the angular positions of the second joints for master-slave systems ($q_{m.2}$ and $q_{s.2}$) as well as the corresponding error between $q_{m.2}$ and $q_{s.2}$ (i.e, $|q_{m.2} - q_{s.2}|$). We can observe that the error between the angular positions for the first joints of master-slave is below 0.6 degs and, the error between the angular positions for the second joints of master-slave is less than 0.65 degs. This indicates that the positions between master and slave are well synchronized within small discrepancies. The convergence rates of entire system via the proposed control technique are tremendously fast according to the fact that the error has almost no transient part. Also, as shown in Fig.9(a) and Fig.9(b), the maximum amplitude of angular position for the first joints and the second ones are approximately ± 60 degs and ± 70 degs respectively. This fact indicates that the maximum error percentages to the maximum amplitudes are approximately 1 % (i.e,0.6/60) and 0.9 % (i.e,0.65/70). To give a clear picture of the movement in Fig.9, the corresponding successive positions of each link for the master and slave devices every 1.4 seconds are illustrated in Fig.10. Particularly, Fig.10(f) represents the consecutive

TABLE 1. Average of estimated dead-zone parameters for four estimates.

parameters	master	parameters	slave	
$m_{m.1}{}^{(+)}$	0.841	$m_{s.1}{}^{(+)}$	0.842	motor attached to the 1st joint
$m_{m.1}{}^{(-)}$	0.842	$m_{s.1}{}^{(-)}$	0.831	
$m_{m.2}{}^{(+)}$	0.81	$m_{s.2}{}^{(+)}$	0.815	motor attached to the 2nd joint
$m_{m.2}{}^{(-)}$	0.601	$m_{s.2}{}^{(-)}$	0.615	
$h_{m.1}{}^{(+)}$	13.8	$h_{s.1}{}^{(+)}$	14.1	motor attached to the 1st joint
$h_{m.1}{}^{(-)}$	15.25	$h_{s.1}{}^{(-)}$	15.15	
$h_{m.2}{}^{(+)}$	13.1	$h_{s.2}{}^{(+)}$	13.4	motor attached to the 2nd joint
$h_{m.2}{}^{(-)}$	5.7	$h_{s.2}{}^{(-)}$	5.78	

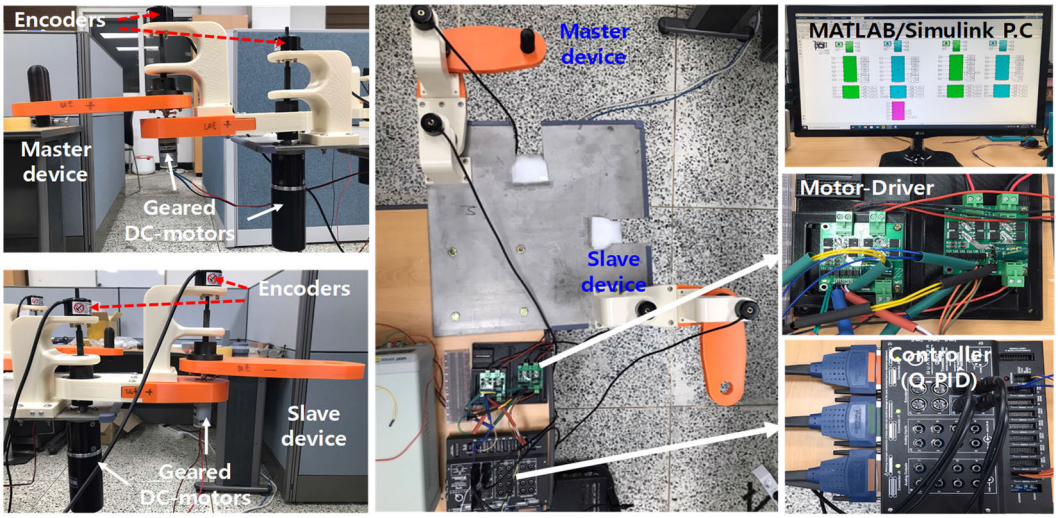

FIGURE 5. Experimental setup for the 2-D.O.F master-slave manipulators together with controller and P.C monitor.

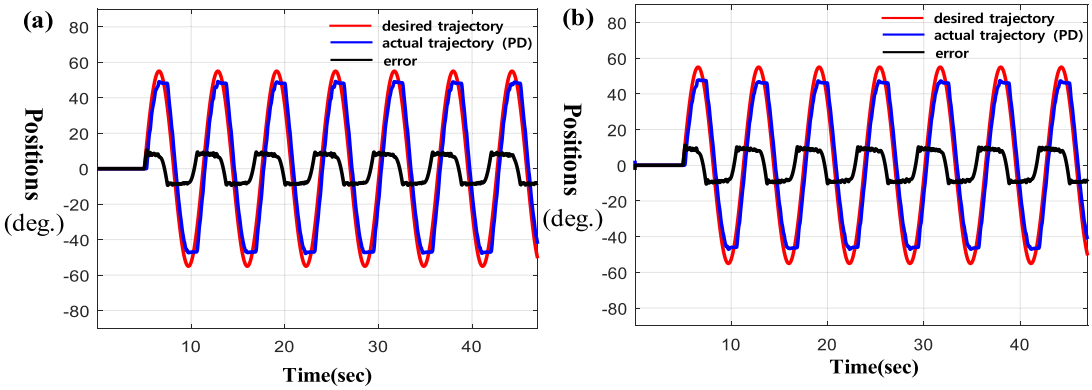

FIGURE 6. Desired trajectory of each joint in the master-slave manipulators for estimating the dead-zone parameters ((a) the 1st joint of master device and (b) the 2nd joint of master device).

movements from 7.5s to 8.9s while Fig.10(g) does the successive positions from 8.9s to 10.3s

Furthermore, Fig.11 includes the comparison between the case w IDZ and the one w/o IDZ. Here, it is executed in the sequential manner that the SMC w/o IDZ (i.e, as indicated by IDZ off in Fig.12) is applied to the system before 25 secs and then the SMC w IDZ (i.e, IDZ on in Fig.12) is activated after 25 secs. Therefore, it can be clearly seen that the maximum errors w/o IDZ are about 6 degs for the first joints and 9 degs for the second joints, respectively. On the other hands, it is observed from both Fig.11(b) and Fig.11(d) that the maximum errors between the master and

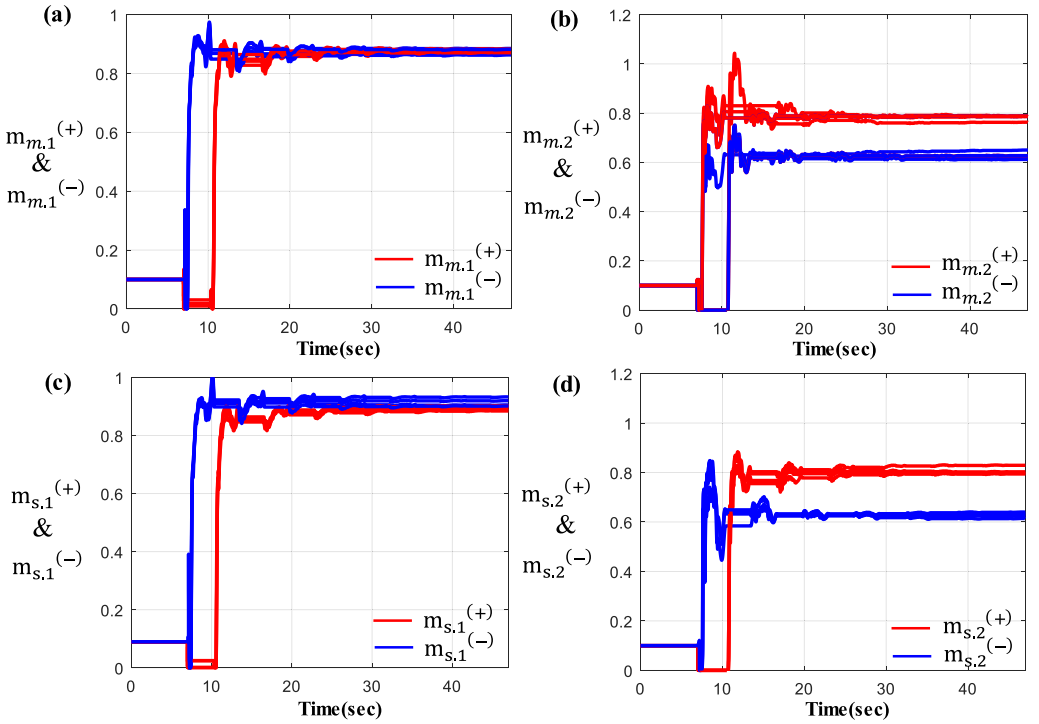

FIGURE 7. Estimated results of the distorted slopes $m_{i,j}^{(\pm)}$ ((a) the distorted slope for the 1st motor of master device ($m_{m.1}^{(\pm)}$), (b) the distorted slope for the 2nd motor of master device ($m_{m.2}^{(\pm)}$), (c) the distorted slope for the 1st motor of slave device ($m_{s.1}^{(\pm)}$) and (d) the distorted slope for the 2nd motor of slave device ($m_{s.2}^{(\pm)}$)).

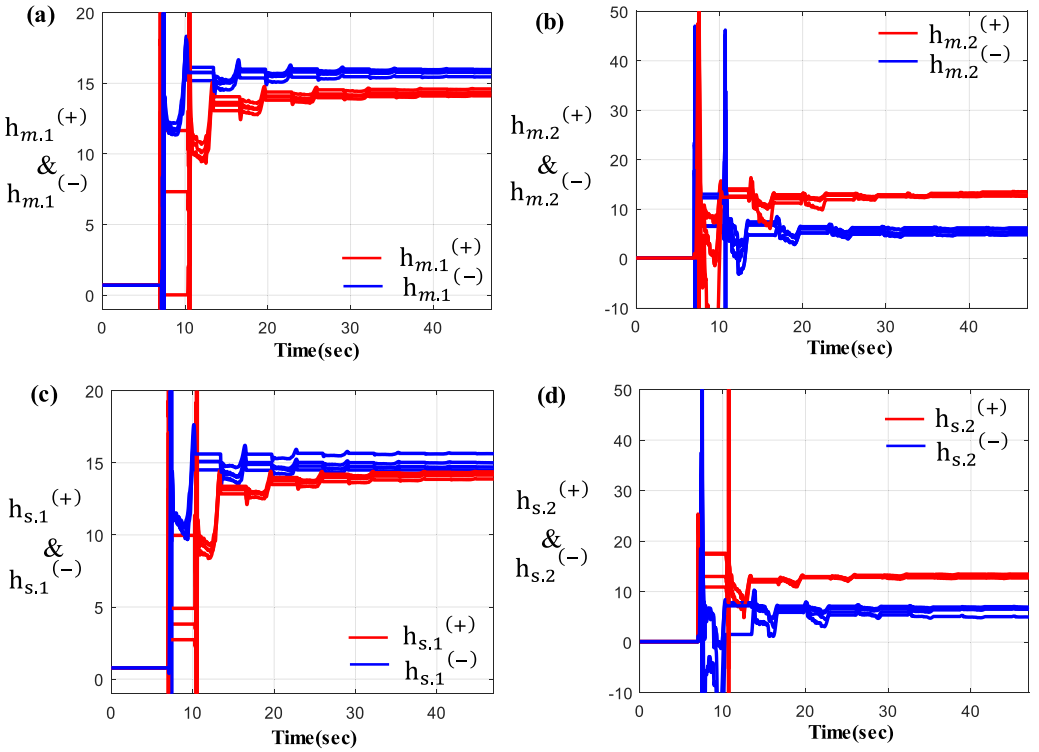

FIGURE 8. Estimated results of the distorted offsets $h_{i,j}^{(\pm)}$ (a) the distorted offset for the 1st motor of master device ($h_{m.1}^{(\pm)}$), (b) the distorted offset for the 2nd motor of master device ($h_{m.2}^{(\pm)}$), (c) the distorted offset for the 1st motor of slave device ($h_{s.1}^{(\pm)}$) and (d) the distorted offset for the 2nd motor of slave device ($h_{s.2}^{(\pm)}$).

slave are 0.5 degs and 0.6 degs after the IDZ is turned on. This implies that the errors have been reduced by almost 92% due to the action of IDZ. The results in Fig.11 clearly illustrate the advantages of IDZ, especially for manipulators

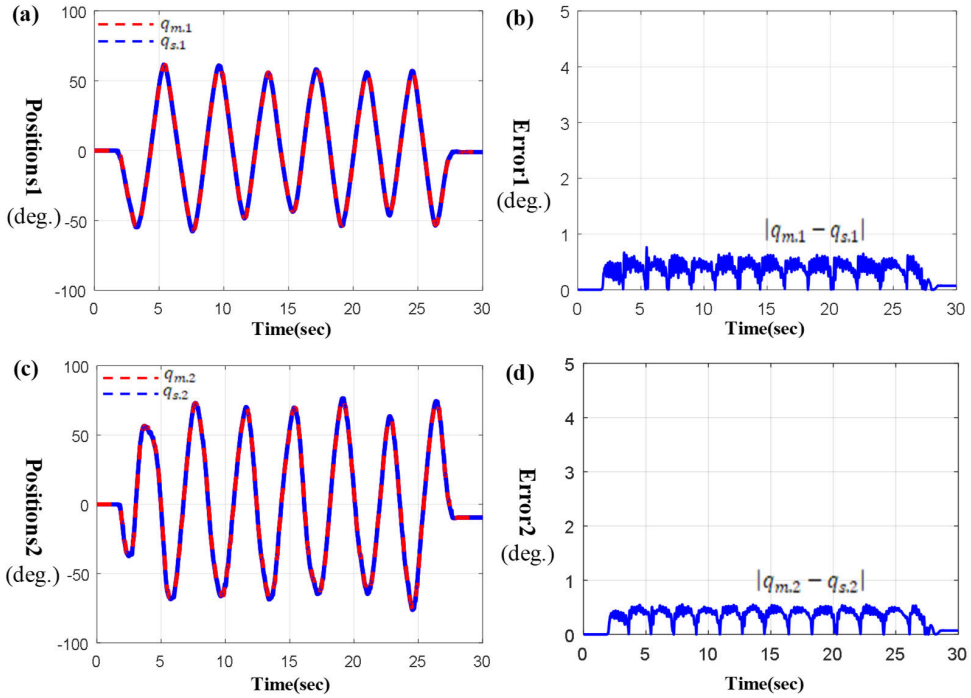

FIGURE 9. Performances of inverse dead-zone based sliding mode control with a communication delay 5 *ms* (a) Angular positions of the 1st joints for master-slave system($q_{m.1}$ and $q_{s.1}$), (b) Error between $q_{m.1}$ and $q_{s.1}$ (i.e, $|q_{m.1} - q_{s.1}|$), (c) Angular positions of the 2nd joints for master-slave system($q_{m.2}$ and $q_{s.2}$) and (d) Error between $q_{m.2}$ and $q_{s.2}$ (i.e, $|q_{m.2} - q_{s.2}|$).

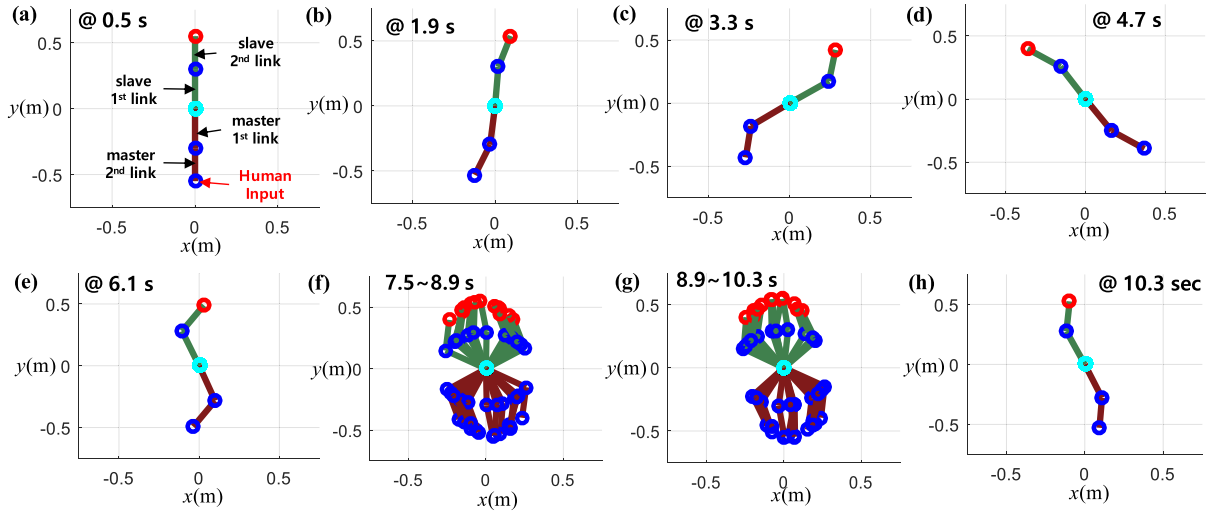

FIGURE 10. Successive positions of each link for the master and slave devices every 1.4 seconds for Fig.9 ((a) positions at 0.5 s, (b) positions at 1.9 s, (c) positions at 3.3 s, (d) positions at 4.7 s, (e) positions at 6.1 s, (f) successive positions from 7.5s to 8.9 s, (g) successive positions from 8.9s to 10.3s, and (h) positions at 10.3 s).

with strong dead-zone characteristics. Also, Fig.12 displays the overall rates of system, indicating $|\dot{q}_{m.1} + \dot{q}_{s.1}|/2$ and $|\dot{q}_{m.2} + \dot{q}_{s.2}|/2$ (i.e, $\dot{\boldsymbol{q}}_{\boldsymbol{Lock}}$) subject to the results of Fig.9. It can be seen that those rates are bounded after 7 secs and this is intended by the proposed control law in (29) through (33).

Therefore, we see that the proposed technique shows the excellence in the precise angular position control of the master-slave manipulators, based on the results of Fig.9 and Fig.11.

Fig.13 demonstrates the torque synchronization of the end-effectors between master and slave systems (i.e, T_h vs. T_E) when the slave is contacted with a passive and firm object.

Here, without using any sensors, T_h and T_E are approximately computed by,

$$T_h = M_{m.21}(\boldsymbol{q_m})\ddot{q}_{m.1} + M_{m.22}(\boldsymbol{q_m})\ddot{q}_{m.2} + C_{m.21}(\boldsymbol{q_m}, \dot{\boldsymbol{q}}_{\boldsymbol{m}})\dot{q}_{m.1} + C_{m.22}(\boldsymbol{q_m}, \dot{\boldsymbol{q}}_{\boldsymbol{m}})\dot{q}_{m.2} - \mathrm{DZ}_{m.2}(\tau_{m.2}) \quad (50)$$

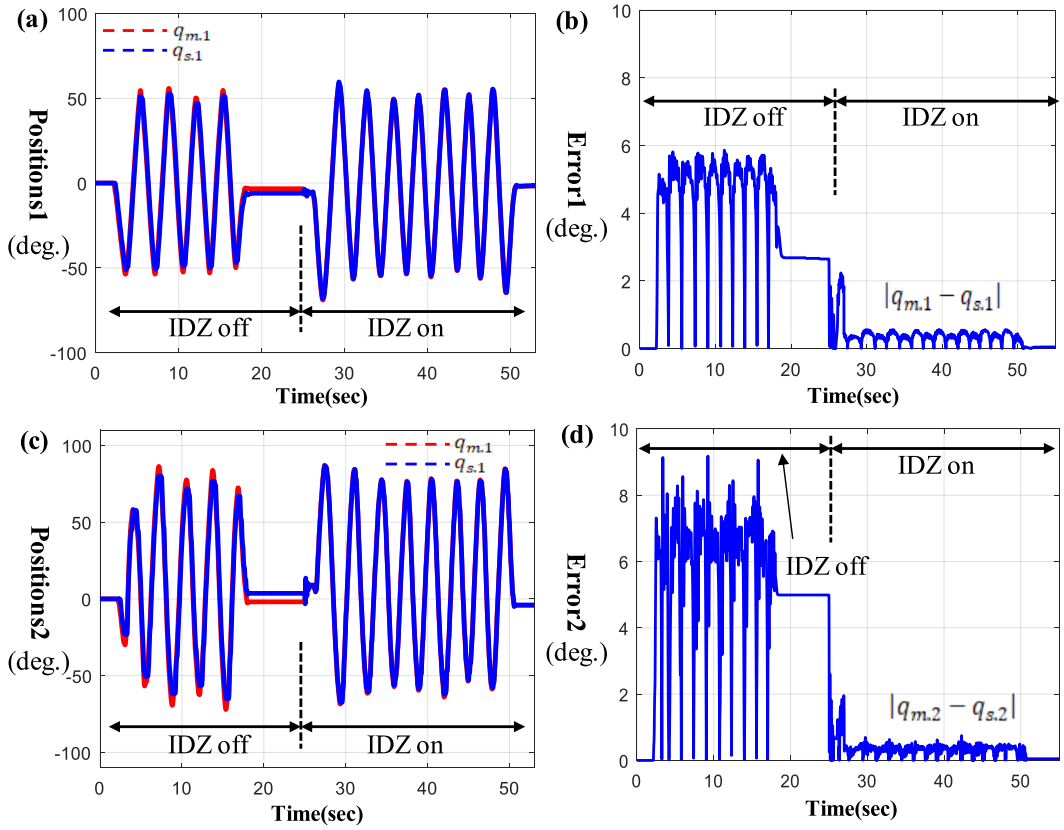

FIGURE 11. Performance comparison between sliding mode control w/o IDZ and the one w IDZ with a communication delay 5 *ms* (a) Positions of the 1st joints for master-slave system($q_{m.1}$ and $q_{s.1}$), (b) Error between $q_{m.1}$ and $q_{s.1}$ (i.e, $|q_{m.1} - q_{s.1}|$), (c) Positions of the 2nd joints for master-slave system($q_{m.2}$ and $q_{s.2}$) and (d) Error between $q_{m.2}$ and $q_{s.2}$ (i.e, $|q_{m.2} - q_{s.2}|$).

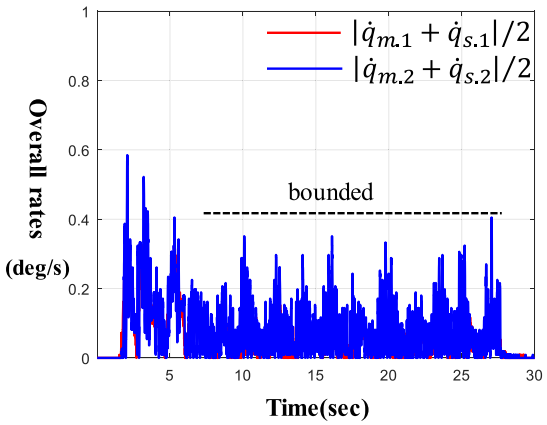

FIGURE 12. Overall rate of system (i.e, $\dot{q}_{Lock}$).

$$\begin{aligned} \mathrm{T}_E = {} & M_{s.21}(\boldsymbol{q}_s)\ddot{q}_{s.1} + M_{s.22}(\boldsymbol{q}_s)\ddot{q}_{s.2} + C_{s.21}(\boldsymbol{q}_s, \dot{\boldsymbol{q}}_s)\dot{q}_{s.1} \\ & + C_{s.22}(\boldsymbol{q}_s, \dot{\boldsymbol{q}}_s)\dot{q}_{s.2} - \mathrm{DZ}_{s.2}\,(\tau_{s.2}) \end{aligned} \tag{51}$$

Fig.13(a) and Fig.13(b) indicate an actual master device with a human operator and actual slave device contacting an object. Also, Fig.13(c) and Fig.13(e) represent the torque synchronization between master and slave systems under the control w/o IDZ and the one w IDZ, respectively. Furthermore, Fig.13(d) and Fig.13(f) contain the corresponding errors between master and slave for Fig.13(c) and Fig.13(e). Regardless of the presence of IDZ, we can see that the torques T_h and T_E are acceptably synchronized as shown in the results of Fig.13(c) and Fig.13(e). However, comparing Fig.13(d) with Fig.13(f), it can be seen that the addition of IDZ actually assists the torque synchronization between master and slave devices resulting in reducing the difference by 50% approximately. This supports that the action of IDZ can reduce not only the position errors but also the torque ones.

Fig.14 shows the effect of communication delay for the position synchronization between master and slave systems. Specifically, the performance of proposed technique based on three different communication delays, 5 *ms*, 10 *ms*, and 15 *ms*, are explored. It is apparent that the angular error between the joints increase as the delay does. With the worst case scenario (i.e, 15 *ms*), the maximum errors are respectively 1.2 degs for the first joints and 2.1 degs for the second joints. Despite such discrepancy, we can see that the states of systems are yet bounded and the proposed technique guarantees a certain level of tele-presence performance

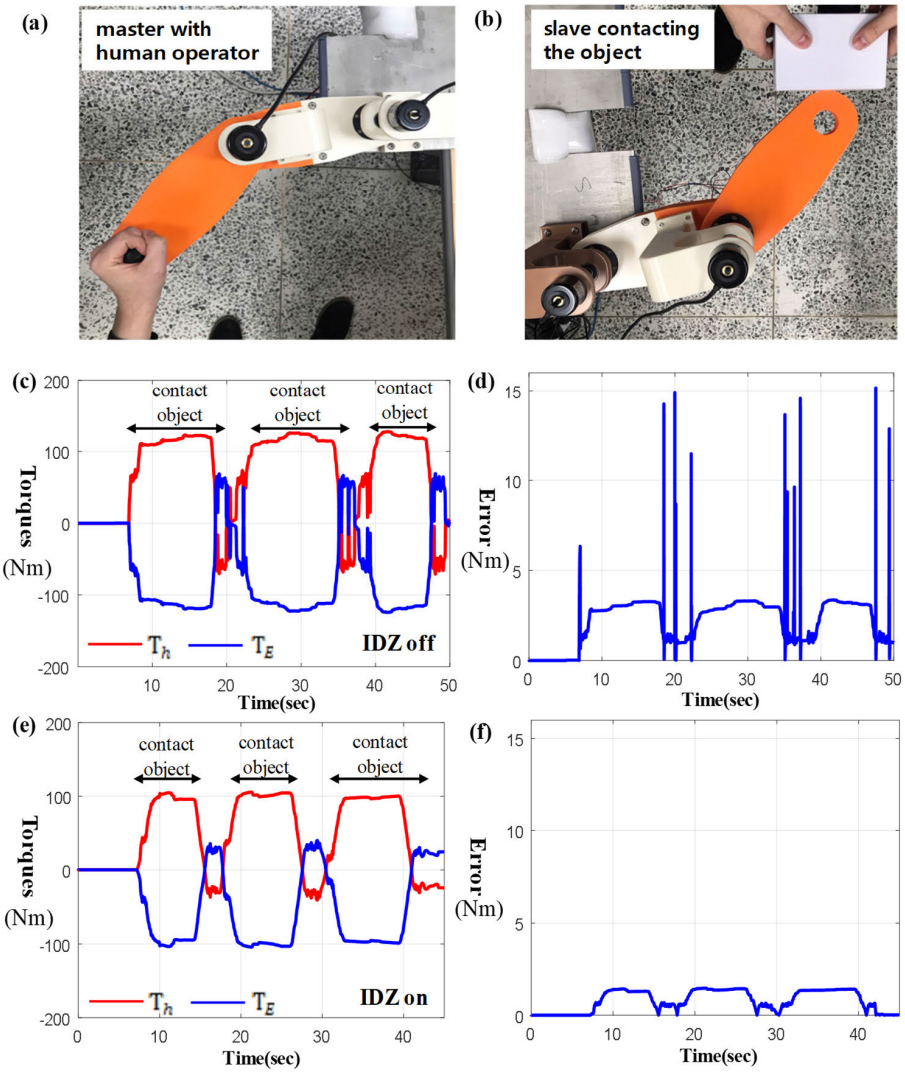

FIGURE 13. Torque synchronization of the end-effectors between master and slave systems with a communication delay 10 *ms* (a) actual master device w human operator, (b) actual slave device contacting an object, (c) Torque synchronization between master and slave systems (IDZ off), (d) Corresponding error of (c), (e) Torque synchronization between master and slave systems (IDZ on), and (f) Corresponding error of (e).

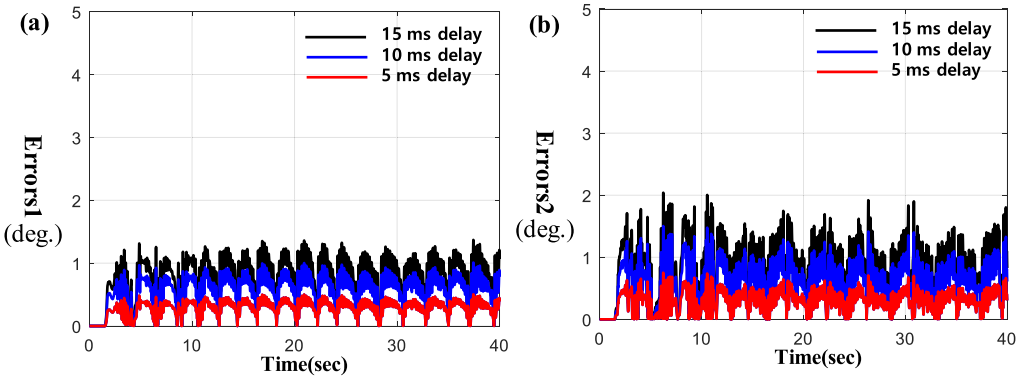

FIGURE 14. Effect of communication delay (a) Errors between $q_{m.1}$ and $q_{s.1}$ (i.e, $|q_{m.1} - q_{s.1}|$) and (b) Errors between $q_{m.2}$ and $q_{s.2}$ (i.e, $|q_{m.2} - q_{s.2}|$).

VI. CONCLUSION

This study proposed the control strategy to compensate the dead-zone effect of actuators for the precise synchronous control between the master and the slave, which has not been thoroughly investigated from other studies. Specifically, we set-forth a two-stage approach that conducting the

estimation of the primary dead-zone parameters in the first stage and the control of the system using the estimated parameters in the first stage. It is found that the estimation of dead-zone parameters is successfully achieved via the proposed method. Eventually, it enables us to achieve that the maximum angular position errors between master and slave devices have been reduced by almost 85 percents compared to the normal operation w/o the action of IDZ. Also, the control systems presented here actually assist the torque synchronization of the end-effectors between master and slave devices under 15 msec. communication delay. This work will be a valuable asset for those who wish to accurately control the synchronization between master-slave systems with uncertain dead-zone characteristics such as the industrial multiple D.O.F robot manipulators actuated via the cost-effective geared actuator.

REFERENCES

[1] A. K. Bondhus, K. Y. Pettersen, and H. Nijmeijer, "Master-slave synchronization of robot manipulators: Experimental results," *IFAC Proc. Volumes*, vol. 38, no. 1, pp. 367–372, 2005.
[2] T. Chen, D. Zhao, and Z. Zhang, "Design of the master-slave manipulators system and research on the bilateral control strategy," in *Proc. 7th World Congr. Intell. Control Autom.*, Chongqing, China, 2008, pp. 9049–9054, doi: 10.1109/WCICA.2008.4594360.
[3] R. Seifabadi, S. M. Rezaei, S. Shiry, M. Saadat, M. Zarei-Nejad, K. Razi, and H. Habibollahi, "Passive bilateral control of a teleoperation system considering hysteresis nonlinearity of slave robot," in *Haptics: Perception, Devices and Scenarios* (Lecture Notes in Computer Science), vol. 5024, M. Ferre, Ed. Berlin, Germany: Springer, 2008, doi: 10.1007/978-3-540-69057-3_9.
[4] J.-H. Ryu, D.-S. Kwon, and B. Hannaford, "Stable teleoperation with time-domain passivity control," *IEEE Trans. Robot. Autom.*, vol. 20, no. 2, pp. 365–373, Apr. 2004, doi: 10.1109/TRA.2004.824689.
[5] D. J. Lee and P. Y. Li, "Passive bilateral feedforward control of linear dynamically similar teleoperated manipulators," *IEEE Trans. Robot. Autom.*, vol. 19, no. 3, pp. 443–456, Jun. 2003.
[6] D. J. Lee and P. Y. Li, "Passive bilateral control and tool dynamics rendering for nonlinear mechanical teleoperators," *IEEE Trans. Robot.*, vol. 21, no. 5, pp. 936–951, Oct. 2005.
[7] D. Lee and M. W. Spong, "Passive bilateral teleoperation with constant time delay," *IEEE Trans. Robot.*, vol. 22, no. 2, pp. 269–281, Apr. 2006.
[8] A. Aziminejad, M. Tavakoli, R. V. Patel, and M. Moallem, "Transparent time-delayed bilateral teleoperation using wave variables," *IEEE Trans. Control Syst. Technol.*, vol. 16, no. 3, pp. 548–555, May 2008, doi: 10.1109/TCST.2007.908222.
[9] X. Li, "Study on master-slave control method using load force and impedance identifiers for tele-operated hydraulic construction robot," *Appl. Mech. Mater.*, vols. 29–32, pp. 2170–2175, Aug. 2010, doi: 10.4028/www.scientific.net/amm.29-32.2170.
[10] R. Tang, "Sliding mode control scheme for tele-operation manipulator," *Appl. Mech. Mater.*, vols. 246–247, pp. 842–846, Dec. 2012, doi: 10.4028/www.scientific.net/amm.246-247.842.
[11] Q. Han, L. Hao, H. Zhang, and B. Wen, "Achievement of chaotic synchronization trajectories of master–slave manipulators with feedback control strategy," *Acta Mechanica Sinica*, vol. 26, no. 3, pp. 433–439, Jun. 2010, doi: 10.1007/s10409-010-0340-9.
[12] T. Wang, B. Pan, Y. Fu, S. Wang, and Y. Ai, "Design of a new haptic device and experiments in minimally invasive surgical robot," *Comput. Assist. Surg.*, vol. 22, no. 1, pp. 240–250, Oct. 2017.
[13] H. Kim, M. Hwang, D. Baek, and D.-S. Kworr, "Robust trajectory tracking of master-slave surgery robot system based on PD with integral sliding mode control," in *Proc. 15th Int. Conf. Ubiquitous Robots (UR)*, Honolulu, HI, USA, Jun. 2018, pp. 48–52, doi: 10.1109/URAI.2018.8441891.
[14] Z. Li and C.-Y. Su, "Neural-adaptive control of single-master–multiple-slaves teleoperation for coordinated multiple mobile manipulators with time-varying communication delays and input uncertainties," *IEEE Trans. Neural Netw. Learn. Syst.*, vol. 24, no. 9, pp. 1400–1413, Sep. 2013, doi: 10.1109/TNNLS.2013.2258681.
[15] K. Kallu, J. Wang, S. Abbasi, and M. Lee, "Estimated reaction force-based bilateral control between 3DOF master and hydraulic slave manipulators for dismantlement," *Electronics*, vol. 7, no. 10, p. 256, Oct. 2018.
[16] L. Li, H. Yang, and J. Liu, "Bilateral coordination control of flexible master–slave manipulators using a partial differential equation model," *J. Vib. Control*, vol. 27, nos. 13–14, pp. 1561–1572, Aug. 2020, doi: 10.1177/1077546320945472.
[17] Z. Chen, F. Huang, C. Yang, and B. Yao, "Adaptive fuzzy backstepping control for stable nonlinear bilateral teleoperation manipulators with enhanced transparency performance," *IEEE Trans. Ind. Electron.*, vol. 67, no. 1, pp. 746–756, Jan. 2020, doi: 10.1109/TIE.2019.2898587.
[18] Z. Chen, F. Huang, W. Sun, J. Gu, and B. Yao, "RBF-neural-network-based adaptive robust control for nonlinear bilateral teleoperation manipulators with uncertainty and time delay," *IEEE/ASME Trans. Mechatronics*, vol. 25, no. 2, pp. 906–918, Apr. 2020, doi: 10.1109/TMECH.2019.2962081.
[19] Y. Ji, D. Liu, and Y. Guo, "Adaptive neural network based position tracking control for dual-master/single-slave teleoperation system under communication constant time delays," *ISA Trans.*, vol. 93, pp. 80–92, Oct. 2019, doi: 10.1016/j.isatra.2019.03.019.
[20] G. Peng, C. L. P. Chen, W. He, and C. Yang, "Neural-learning-based force sensorless admittance control for robots with input deadzone," *IEEE Trans. Ind. Electron.*, vol. 68, no. 6, pp. 5184–5196, Jun. 2021, doi: 10.1109/TIE.2020.2991929.
[21] T. Kara and İ. Eker, "Nonlinear modeling and identification of a DC motor for bidirectional operation with real time experiments," *Energy Convers. Manage.*, vol. 45, pp. 1087–1106, May 2004.
[22] J. O. Jang, "A deadzone compensator of a DC motor system using fuzzy logic control," *IEEE Trans. Syst., Man, Cybern. C, Appl. Rev.*, vol. 31, no. 1, pp. 42–48, Feb. 2001, doi: 10.1109/5326.923267.
[23] N. J. Ahmad, H. K. Ebraheem, M. J. Alnaser, and J. M. Alostath, "Adaptive control of a DC motor with uncertain deadzone nonlinearity at the input," in *Proc. Chin. Control Decis. Conf. (CCDC)*, Mianyang, China, May 2011, pp. 4295–4299, doi: 10.1109/CCDC.2011.5968982.
[24] X. Liu, W. Jiang, and X.-C. Dong, "Nonlinear adaptive control for dynamic and dead-zone uncertainties in robotic systems," *Int. J. Control, Autom. Syst.*, vol. 15, no. 2, pp. 875–882, Apr. 2017, doi: 10.1007/s12555-015-0449-5.
[25] G. Galuppini, L. Magni, and D. M. Raimondo, "Model predictive control of systems with deadzone and saturation," *Control Eng. Pract.*, vol. 78, pp. 56–64, Sep. 2018.
[26] J. Peng and R. Dubay, "Identification and adaptive neural network control of a DC motor system with dead-zone characteristics," *ISA Trans.*, vol. 50, no. 4, pp. 588–598, 2011.
[27] J. H. P. Cruz, J. D. J. R. Avila, J. L. Flores, and E. Rangel, "Control of uncertain plants with unknown deadzone via differential neural networks," *IEEE Latin Amer. Trans.*, vol. 13, no. 7, pp. 2085–2093, Jul. 2015, doi: 10.1109/TLA.2015.7273762.

DAEYI JUNG received the Ph.D. degree from the Department of Mechanical Engineering, University of Tennessee, Knoxville, TN, USA, in 2012. He had worked as a Senior Researcher with Samsung Electronics and Hyundai-motors for several years and has been with Kunsan National University (KSNU), South Korea, since 2017. He is currently an Associate Professor with the Department of Mechanical Engineering, KSNU. His research interest includes the controls and analysis of nonlinear systems.

JONGYEON JEON received the bachelor's degree from the Department of Mechanical Energy Engineering, Kunsan National University (KSNU), South Korea, in 2019, and the master's degree from the Department of Mechanical Engineering, KSNU. His research interest includes the controls of nonlinear systems.